



Contents lists available at SciVerse ScienceDirect

## Acta Biomaterialia

journal homepage: [www.elsevier.com/locate/actabiomat](http://www.elsevier.com/locate/actabiomat)

# Moisture based three-dimensional printing of calcium phosphate structures for scaffold engineering

A. Butscher<sup>a,b,\*</sup>, M. Böhner<sup>a</sup>, N. Doebelin<sup>a</sup>, L. Galea<sup>a</sup>, O. Loeffel<sup>a</sup>, R. Müller<sup>b</sup>

<sup>a</sup>RMS Foundation, Bismattstrasse 12, CH-2544 Bettlach, Switzerland

<sup>b</sup>Institute for Biomechanics, ETH Zurich, Wolfgang-Pauli-Strasse 10, CH-8093 Zurich, Switzerland

## ARTICLE INFO

### Article history:

Received 27 July 2012

Received in revised form 26 September 2012

Accepted 5 October 2012

Available online 13 October 2012

### Keywords:

Three-dimensional printing (3DP)

Calcium phosphate

Tissue engineering

Synthetic bone substitute

## ABSTRACT

Powder based three-dimensional printing (3DP) allows great versatility in material and geometry. These characteristics make 3DP an interesting method for the production of tissue engineering scaffolds. However, 3DP has major limitations, such as limited resolution and accuracy, hence preventing the widespread application of this method. In order to reduce these limitations deeper understanding of the complex interactions between powder, binder and roller during 3DP is needed. In the past a lot of effort has been invested to optimize the powder properties for 3DP for a certain layer thickness. Using a powder optimized for an 88  $\mu\text{m}$  layer thickness, this study systematically quantifies the surface roughness and geometrical accuracy in printed specimens and assesses their variation upon changes of different critical parameters such as the moisture application time (0, 5, 10 and 20 s), layer thickness (44 and 88  $\mu\text{m}$ ) and the number of specimens printed per batch (6 and 12). A best surface roughness value of 25  $\mu\text{m}$  was measured with a moisture application time (using a custom made moisture application device mounted on a linear stage carrying the print head) of 5 s and a layer thickness of 44  $\mu\text{m}$ . Geometrical accuracy was generally higher for the 88  $\mu\text{m}$  thick layer, due to a less critical powder bed stability. Moisture application enabled 3DP of a 44  $\mu\text{m}$  thick layer and improved the accuracy even for a powder initially optimized for 88  $\mu\text{m}$ . Moreover, recycling of the humidified powder was not only possible but, in terms of reactivity, even beneficial. In conclusion, moisture-based 3DP is a promising approach for high resolution 3DP of scaffolds.

© 2012 Acta Materialia Inc. Published by Elsevier Ltd. All rights reserved.

## 1. Introduction

Three-dimensional printing (3DP) is a versatile solid, free-form fabrication (SFF) technique with high potential for scaffold engineering. The flexibility that 3DP offers is outstanding not only in terms of geometrical flexibility (free-form) but also in terms of the broad materials choice [1]. Provided the desired material exists in powder form of appropriate size, almost any material can be synthesized by 3DP. This flexibility opens up totally new approaches within regenerative medicine, such as 3-D printed patient-specific models based on calcium phosphate (CaP) powders for maxillofacial bone regeneration [2–4]. While CaP is well established as a synthetic bone substitute biomaterial [5–8], scaffolds built up by 3DP of CaP powders provide a unique geometrical flexibility that cannot be achieved by traditional manufacturing processes. Furthermore, the inherent rough powder surface in 3DP is reported to enhance cell adhesion [9–12].

However, as high as the potential of 3DP is, the challenges are and will be large. The geometrical flexibility is restricted by the limited resolution (the typical layer thickness is close to 100  $\mu\text{m}$ ). While for certain industrial 3DP applications this resolution might be sufficient, it is critical when building up tiny and complex geometries for scaffold engineering. The definition of an adequate pore size is still a matter of debate [13]. However, it is generally reported to be in the range 50–1000  $\mu\text{m}$  [14–16]. While high resolution free-form fabrication methods (e.g. stereolithography) allow the production of pores in the lower size range, only macropores larger than 500  $\mu\text{m}$  can be currently achieved using 3DP [1].

The resolution and accuracy of 3DP are determined by multiple factors, such as print head resolution, precision of the linear stage positioning, binder drop volume, binder–powder interaction, particle size and, last but not least, layer thickness. Unfortunately, efforts to determine these effects are often hampered by the limitations set by commercial printers. Nevertheless, even if a printed specimen meets the required accuracy, depowdering (removing loose particles around and within the printed body) is critical.

In order to achieve a breakthrough in 3DP for scaffold engineering, accuracy (the mismatch between the model and the 3DP specimen) and resolution (smallest feature size) need to be

\* Corresponding author at: RMS Foundation, Bismattstrasse 12, CH-2544 Bettlach, Switzerland. Tel.: +41 32 644 1400; fax: +41 32 644 1176.

E-mail address: [andre.butscher@rms-foundation.ch](mailto:andre.butscher@rms-foundation.ch) (A. Butscher).

substantially improved [17]. In a previous work the interplay between powder properties and final printing outcome was investigated in detail [18]. It was demonstrated that particle properties such as particle size, flowability, wettability and compaction rate could be optimized and thus determine the best possible 3DP outcome for a certain layer thickness. In particular, it was shown that there was an optimum range of powder flowability related to the powder mean particle size. When the powder was too fine flowability was too low, thus resulting in smearing and poor resolution. When the powder was too coarse flowability was too high, leading to powder bed instability and again poor resolution.

Currently the resolution of 3DP is mainly limited by too large a layer thickness, typically in the region of 100  $\mu\text{m}$ . This provokes the so-called stair stepping effect [19], which has a significant impact on the surface texture of printed solids. While stair stepping is predominant for curved surfaces, a similar effect is detected on vertical surfaces due to small lateral shifts occurring between superimposed layers. A smaller layer thickness is thus mandatory. However, the ideal 3DP powder should have a mean diameter greater than 20  $\mu\text{m}$  because below this value interparticular forces dominate gravitational forces [20]. Furthermore, the layer thickness should be at least three particles thick, due to issues of powder flow and spreadability [21]. In other words, there is a conflict between higher accuracy on the one hand and 3-D printer and powder requirements on the other.

In the literature a few studies have shown that powders smaller than 20  $\mu\text{m}$  can be controlled to a certain degree by plasma coating [22] or lubricants [23]. However, these changes, in connection with a change in particle size [24], have an impact on the wetting characteristics of the powder. Other studies have shown that layer thicknesses down to 25  $\mu\text{m}$  are possible [25,26], without, however, focussing on the link between layer thickness and printing accuracy. Powder bed stability during deposition of a new layer also becomes a very important issue at low layer thicknesses and small particle sizes. Indeed, since shear forces in the powder bed increase with a decrease in layer thickness, recoating of a new powder layer is not only a complex but critical factor [27,28]. Furthermore, the binder droplets jetted onto the powder bed are more likely to displace small particles than large particles. In order to improve the powder bed stability local application of moisture to the powder bed was chosen. This method has already been mentioned in a few articles by the inventors of 3DP [29,30], however, an in depth understanding of this approach is lacking.

This study aims at systematically analysing the interplay between layer thickness, layer stability and the final quality of the printed specimens. In order to approach the resolution and pore sizes relevant for scaffold engineering layer thicknesses of 88 and 44  $\mu\text{m}$  were selected and compared. Moreover, tests were carried out without and with local moisture application to the top powder layer, in order to enable and improve 3DP with the fine powders necessary for 44  $\mu\text{m}$  layers.

Based on the insights gained it is hoped that 3DP resolution and accuracy can be improved, which in return would lead to the synthesis of more accurate CaP scaffolds.

## 2. Materials and methods

### 2.1. Powders

A home-made  $\alpha$ -tricalcium phosphate ( $\alpha$ -TCP) ( $\alpha$ - $\text{Ca}_3(\text{PO}_4)_2$ ) powder was used.  $\alpha$ -TCP is a more reactive phase than  $\beta$ -TCP and leads to better 3DP results [18]. Furthermore  $\alpha$ -TCP has excellent in vivo behavior [31]. In our approach  $\alpha$ -TCP particles undergo a cement reaction described in detail in Butscher et al. [1]. Briefly, the  $\alpha$ -TCP particles are dissolved by the phosphoric acid print head

jet and brushite crystals precipitate in the resulting solution. Hardening (or particle “binding”) occurs via entanglement of these brushite crystals. Accordingly, and for convenience, the phosphoric acid solution is termed “binder” in this manuscript. Further densification of the reacted powder can be achieved using either heat treatment or improved by a post-hardening regime after printing, also improving the in vivo biological stability [32].

The powder was produced according to a previously published procedure [26] differing only in the use of a lower Ca/P molar ratio (1.45) and slightly higher sintering temperature (1400  $^\circ\text{C}$ ). Briefly, a 0.45:1 M ratio blend of calcium carbonate (CC) powder ( $\text{CaCO}_3$ , Merck, Germany, catalogue No. 102076) and dicalcium phosphate (DCP) powder ( $\text{CaHPO}_4$ , GFS Chemical, USA, catalogue No. 1548) was mixed in a Turbula mixer (Bachofen, Switzerland) for 1 h. After calcining at 900  $^\circ\text{C}$  for 1 h in an LHT 02/16 furnace (Nabertherm, Germany) the powder was cooled to room temperature. The calcined powder was then sieved (AS 200, Retsch, Switzerland) through a 0.125 mm sieve, sintered at 1400  $^\circ\text{C}$  for 4 h, and then removed from the furnace to quench the powder in air. Finally, the sintered powder was broken in a jaw crusher (BB51, Retsch, Germany), milled and separated to obtain the desired particle fraction (according to Butscher et al. [18]).

### 2.2. 3D printer

A commercial 3-D printer (Zprinter 310plus, Z Corp., Burlington, USA) was used. The printer was adapted to meet the requirements of this study. Firstly, the feed and build reservoirs were reduced to areas of 60  $\times$  90 and 50  $\times$  80 mm, respectively, to enable 3DP with smaller powder amounts and thus reduce the time per print and the powder material cost. A layer thickness of 88  $\mu\text{m}$  and a binder/volume ratio of 0.28 for the shell and 0.14 for the core of the 3DP using pure 10% phosphoric acid as the binder fluid (or reaction fluid) were taken to be standard parameters. Unfortunately, printing a layer thickness less than 88  $\mu\text{m}$  was not possible with the commercial version of the printer used in this study. Therefore, a relatively simple mechanical approach was used to halve the layer thickness. To this end the linear actuators used to control the vertical position of the feed and build volume were disassembled and the original lead screws with an outer diameter of 9.525 mm and a thread lead of 2.54 mm were replaced by an equivalent lead screw and matching threaded sleeve with half the thread lead. To print a layer thickness of 44  $\mu\text{m}$  the binder/volume ratio was kept the same as mentioned above. The exact layer thickness was determined using a digital displacement gauge (S229 dial gauge, Sylvac, Switzerland) for at least six steps and repeated three times.

Furthermore, a custom made moisture unit was mounted on the linear stage (Fig. 1a). This moisture unit allowed application of moisture via a magnetic inlet valve just before the print head jet applied the binder to the powder bed. Pure water moisture was produced inside a nebulizer (USV 3002, Schulte, Germany) normally used for inhalation therapy. The moisture was applied from the top of the moisture chamber and was sucked away via channels inside the walls of the moisture unit by a ventilation system (Fig. 1b). A custom made control system allowed automated positioning and timing of the moisture unit within the 3DP process.

In order to quantify the effect of different moisture regimes and layer thicknesses simple solids of spheres, cubes, cylinders (Fig. 2a) and pyramids (described later) were generated with the CAD software NX 7.5 (PLM Software, Siemens, Germany) and imported into the 3-D printing software in the .stl (stereolithography) file format. Since the printer was unaware of the hardware changes the models had to be scaled according to the change in linear travel of the actuator. While the sphere represented a critical case concerning powder bed stability, the cube and cylinder, which are less critical,

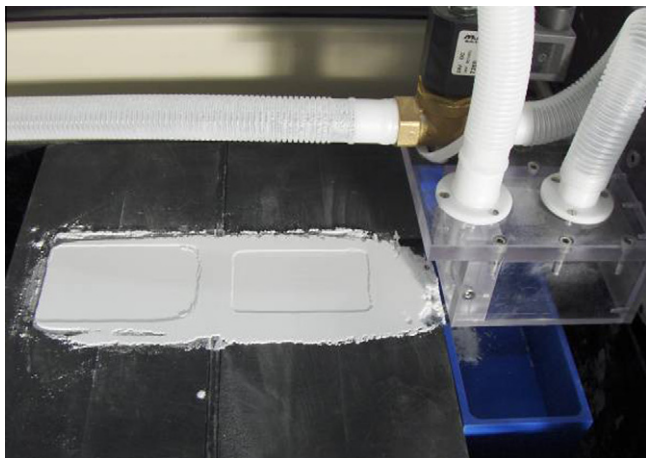


Fig. 1a. Custom made moisture unit mounted on the linear stage.

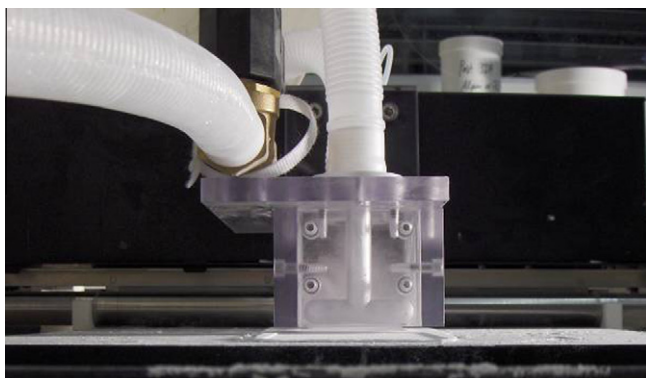


Fig. 1b. Ventilation system removes moisture via channels inside the walls of the moisture unit.

were also included. The printed specimens were then analysed macroscopically.

Pyramids with an overall length/width of 20 mm and four 2 mm steps (Fig. 2b) were printed to quantify surface roughness microscopically by the procedure described below. The same two defined areas on the  $x$  side of the pyramid were always investigated. The  $x$  side was always placed parallel to the powder roller axis in order to account for shear powder bed stability. Roughness was not measured on the  $y$  side of the pyramid because the powder roller moved along the  $y$  direction and, as a result, the  $y$  side should be less critical than the  $x$  side.

Experimentally, three factors were varied and looked at: the moisture regime (0, 5, 10 and 20 s humidification time), the layer thickness (88 and 44  $\mu\text{m}$ ), and the number of printed parts (6-part and 12-part models) (Fig. 3). However, the 20 s humidification time had to be excluded from the statistical analysis, as explained in detail later.

### 2.3. Powder characterization

The powder used in this study was characterized using different methods: (i) laser diffraction to determine the particle size distribution (PSD); (ii) scanning electron microscopy (SEM) to analyse the morphology of the powders; (iii) X-ray diffraction (XRD) to determine the crystalline composition; (iv) isothermal calorimetry to assess the powder reactivity (particularly after humidification);

(v) quantification of flowability using a ring shear tester and a custom method based on funnels of various dimensions.

The PSD of the dry powder was measured by laser diffraction (Helos & Rodos, Sympatec, Germany). Powder dispersion into the air stream prior to laser diffraction measurement was achieved with a vibratory chute.

For SEM (EVO MA 25, Zeiss, Germany) the samples were placed on a sticky carbon tape (SCD 050 Sputter Coater, Baltec, Switzerland) and then sputtered with two thin layers of platinum ( $\sim 10$  nm, sputter time 60 s at 40 mA).

XRD were recorded using a diffractometer (cubiX, Panalytical, The Netherlands) with  $\text{CuK}_{\alpha 1}$  radiation made monochromatic with graphite in the range  $4\text{--}60^\circ 2\theta$ . The quantitative phase composition was determined by Rietveld refinement using the software FullProf.2 k v. 5.0 (<http://www.ill.eu/sites/fullprof/>) [33]. Structural models were taken from Dickens et al. [34] for  $\beta$ -TCP, Sudarsanan et al. [35] for hydroxyapatite, Boudin et al. [36] for  $\beta$ -calcium pyrophosphate and Mathew et al. [37] for  $\alpha$ -TCP. No other phases were identified in the diffraction patterns.

For calorimetry measurements an eight station isothermal calorimeter (TAM AirCement, Thermometric AB, Sweden) was used. For this purpose in every station 2 g of  $\alpha$ -TCP powder and 1 ml of 0.2 M sodium phosphate ( $\text{Na}_2\text{HPO}_4$ , Fluka, Switzerland) solution were placed in sealed 20 ml admix ampoules of a mixing cell and a connected syringe, respectively. When a constant (zero) heat signal was reached (1–2 h after insertion of the mixing cells into the calorimeter) the solution was injected onto the powder and mixed for 15 s with an in situ stirring bar. Measurement continued until a constant thermal signal was reached. Four samples were tested for each moisture regime (0, 5, 10, and 20 s moisture application, see below). Since it was not possible to fully reproduce the reactions taking place during 3DP due to corrosion of the metallic parts of the mixing cell when using phosphoric acid, two approaches were used to measure the potential change in reactivity due to  $\alpha$ -TCP humidification: (i) mixing  $\alpha$ -TCP with sodium phosphate solution; (ii) mixing  $\alpha$ -TCP and monocalcium calcium phosphate monohydrate (MCPM) powder with water. The second approach replaced the sodium phosphate solution with water and the  $\alpha$ -TCP with a mixture of 0.2 g MCPM and 0.3 g  $\alpha$ -TCP to account for the acidic reaction during 3DP. Furthermore, potential surface changes provoked by the interaction between humid air and  $\alpha$ -TCP powder were assessed by SEM.

Achieving reproducible flowability measurements of powders is not a trivial matter [38–40]. Here the two approaches described in Butscher et al. [24] were used. In the first method a ring shear cell (RST-XS, Schulze Schüttgutmesstechnik, Germany) [41] was filled with 30 ml of powder, the pre-shear stress was set to 1500 Pa, and shear stresses of 300, 750, 1200 and 300 N were applied. The measurement was repeated three times for each sample. Flowability was expressed as the so-called flow factor ( $ff_c$ ) [38] defined as the ratio of the consolidation stress  $\sigma_1$  and the compression strength  $\sigma_c$ :

$$ff_c = \frac{\sigma_1}{\sigma_c}$$

Schulze [41] proposed the following classification as a measure of the qualitative flowability ranges:  $ff_c > 10$ , free flowing;  $4 < ff_c < 10$ , easy flowing;  $2 < ff_c < 4$ , cohesive;  $1 < ff_c < 2$ , very cohesive;  $ff_c < 1$ , non-flowing.

The second approach to measure flowability was based on the use of funnels [42]. As described in a previous publication [24], custom made glass funnels (diameter 46 mm, angle  $35^\circ$ ) with different orifices (diameters of 8, 12, 18, 24, 30 and 36 mm) were filled in a reproducible manner and lifted up by hand. If the powder flew out, the procedure was repeated with the next smallest

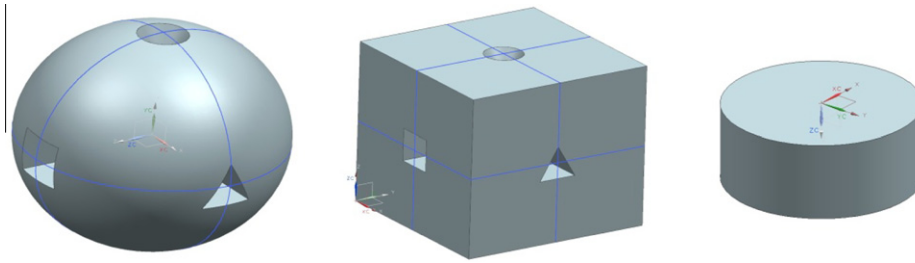


Fig. 2a. Simple solids used as input for accuracy quantification: sphere, cube and disc.

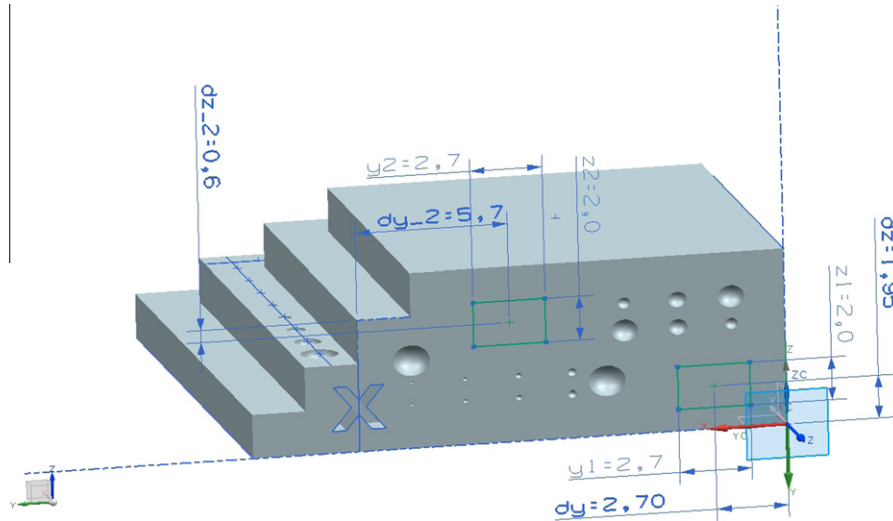


Fig. 2b. Pyramids with four 2 mm steps used to quantify surface roughness in two defined areas (marked with a green rectangle).

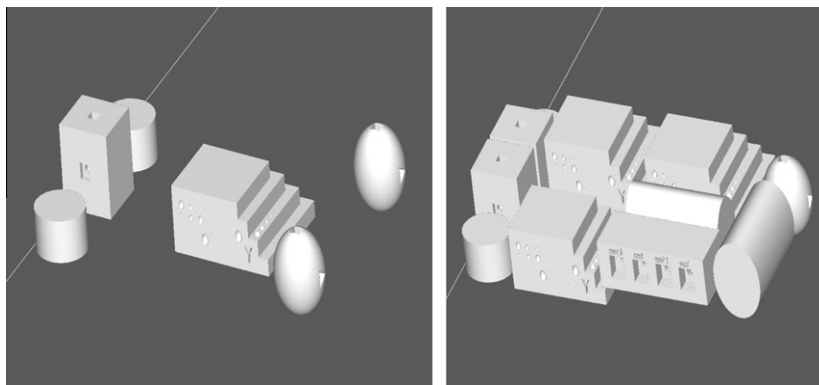


Fig. 3. Visualization of two batch densities used for printing: 6 part (left) and 12 part (right).

diameter. The outcome was a simple but reliable pass/non-pass powder ranking for different cylinder orifices.

The specific surface area (SSA) was determined by nitrogen adsorption (Gemini 2360, Micromeritics, USA), applying the Brunauer–Emmet–Teller (BET) equations. The powder was dried at 130 °C for 3 h in order to remove residual moisture prior to SSA characterization.

Bulk and tapped densities were determined according to standardized test methods [43,44]. For the bulk density a given powder volume was weighed without tapping, while the tapped density powder specimen was first tapped 150 times and then weighed.

#### 2.4. 3DP sample characterization

The surface roughness of two different predefined areas on the  $x$  side of the pyramids (Fig. 2b) was analysed. In order to achieve reproducible results, all specimens were cleaned with compressed air (2.5 bars with a 0.45 mm sterile filter with inlet diameter 4.0 mm, outlet diameter 2.8 mm, Acrodisc CR PTFE, Pall Gelman, USA) for about 5 s and a distance of 10 cm prior to analysis. Special care was taken in specimen handling, with touching of the  $x$  side of the pyramid being avoided. Later each surface was imaged from two different angles (0° and 7°) using SEM in VP mode (60 Pa N<sub>2</sub>

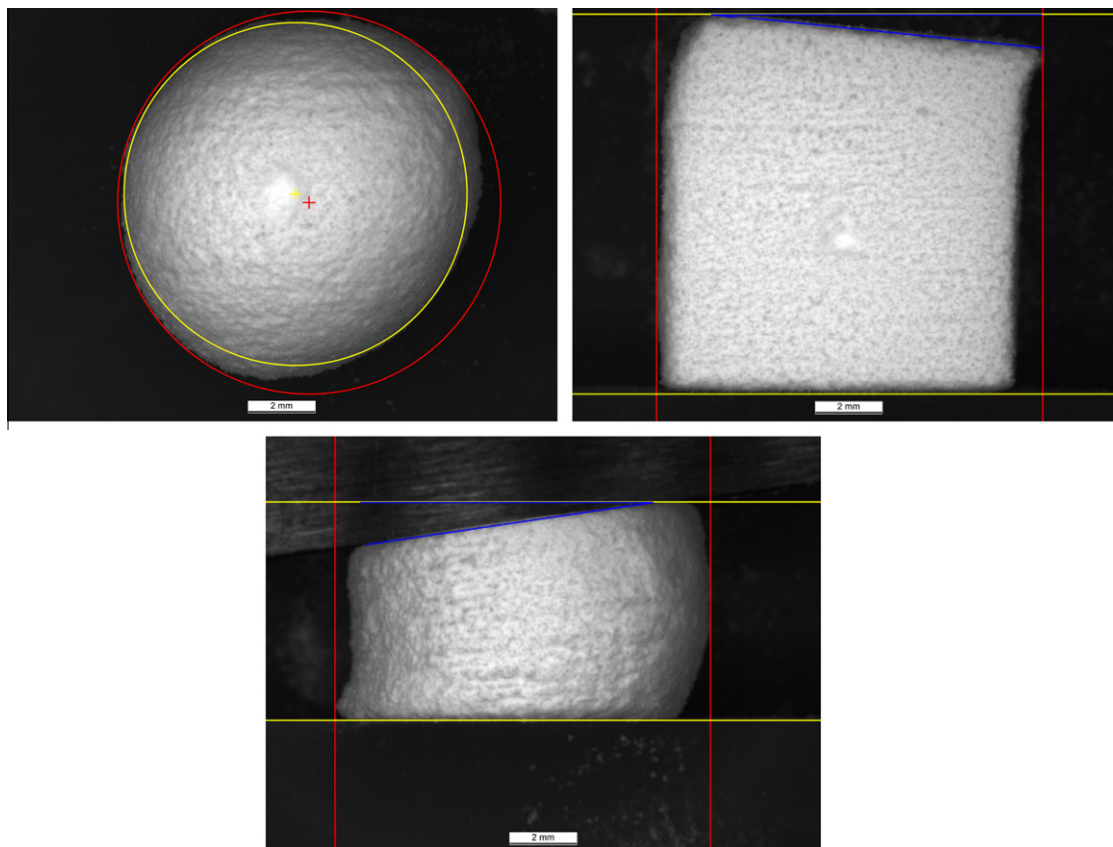


**Fig. 4.** Image analysis for determination of the geometrical accuracy of the printed solids: sphere (above) measuring inner and outer diameter; cube and cylinder (middle and below) measuring height, length and angle.

partial pressure, VPSE detector). Imaging software (MeX V5.1, Alicona Imaging, Austria) was then applied for 3-D surface reconstruction. For that purpose a reference plane was adjusted on the primary profile. Finally, the arithmetic average surface roughness ( $S_a$ ) was calculated, serving as a simple value for roughness quantification.

As a complement to the microscopic roughness analysis, the macroscopic geometry of the 3DP specimen was documented using imaging software (Image Access 11 Premium, release 11.3, Imagic, Switzerland). This was used to account for macroscopic effects due to moisture application and layer thickness neglected by the local roughness measurements. For this purpose the deviations of printed specimens from the original model were compared and if possible quantified. More precisely, the minimal and maximal diameters of the printed spheres were determined. This deviation from the real diameter served as a measure for the aspheric volume and thus the shear powder bed stability. For the cubes and the cylinders a similar approach was taken. To account for shear movement errors due to the recoating of a new powder layer all solids were analysed perpendicular to this shear movement (Fig. 4). Parameters measured for the cylinders and cubes included cylinder height and angle. The height was defined as the maximal distance between the baseline (bottom horizontal reference line) and the highest point, while the angle was measured between the bottom baseline and the top boundary line of the cube or the cylinder (Fig. 4).

### 2.5. Statistics

Statistical analysis was carried out using a multifactorial (ANOVA) analysis. We have set the significance level at  $P < 0.01$ . This

analysis was performed using software written by J. Lemaître (<http://ltp.epfl.ch/page-35623-en.html>).

### 3. Results

An overview and higher magnification of the particle morphology of the  $\alpha$ -TCP reference powder (no humidification) and the same powder after humidification for 20 s are presented in Fig. 5. At low resolution the particles exhibited an irregular shape with predominant sharp edges. Since the smallest were eliminated from the powder, only a low degree of agglomeration could be observed. No morphologically relevant differences could be seen between the different moisture regimes. At high resolution, however, fine crystalline structures were seen in the humidified samples, particularly after 20 s (Fig. 5). This effect was not seen for the  $\alpha$ -TCP reference powder (no humidification).

The powder PSD was monomodal and in good agreement with the SEM images. The mean particle size was  $21.20 \pm 0.09 \mu\text{m}$ . XRD analysis revealed a high level of  $\alpha$ -TCP phase (>95%). Further relevant powder characterizations, such as the SSA and bulk/tapped densities, are presented in Table 1.

Calorimetry measurements are presented in Fig. 6. When  $\alpha$ -TCP reacted with sodium phosphate solution a bimodal or even trimodal curve was measured (Fig. 6a). Interestingly, the intermediate peak (between 0.1 and 1 h) was shifted to shorter times at longer humidification times (Fig. 6b). However, the total amount of heat released during the reaction did not decrease significantly. When  $\alpha$ -TCP was reacted with MCPM and water the reaction was much faster (Fig. 7a). The reaction was complete within 1 h, whereas mixtures of  $\alpha$ -TCP and sodium phosphate solution took several

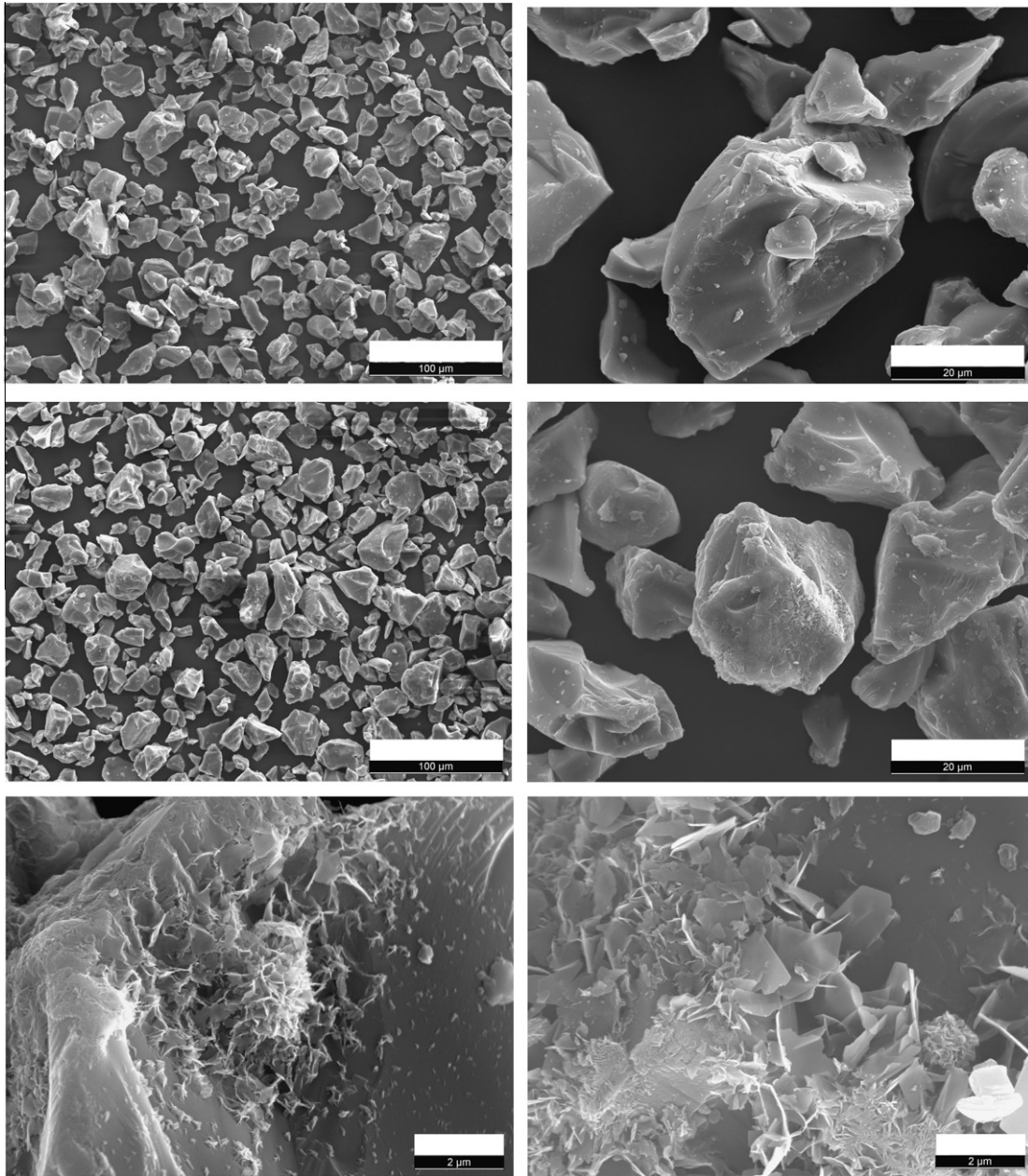


**Fig. 5.** Particle morphology of the  $\alpha$ -TCP powder particles without treatment (above) and after 20 s humidification (middle and below). The white bar indicates a distance of 100  $\mu\text{m}$  (left) and 20  $\mu\text{m}$  (right) for the top and middle, while for the close up below the bar indicates 2  $\mu\text{m}$  (left and right).

**Table 1**  
Powder characterisation: percentiles of particle size distribution ( $d_{10}/d_{50}/d_{90}$ ), flowability results, specific surface area (SSA), bulk and tapped densities, and compaction (ratio of bulk and tapped densities).

	$d_{10}/d_{50}/d_{90}$ ( $\mu\text{m}$ )	$ff_c$	Funnel (mm)	SSA ( $\text{m}^2/\text{g}$ )	$\rho_{\text{Bulk}}$ ( $\text{kg}/\text{m}^3$ )	$\rho_{\text{Tapped}}$ ( $\text{kg}/\text{m}^3$ )	$\rho_{\text{Tapped}}/\rho_{\text{Bulk}}$
$\alpha$ -TCP	9/21/37	$5.3 \pm 0.1$	24	$0.28 \pm 0.04$	$974 \pm 11$	$1399 \pm 4$	1.44

days to react. A significant increase in the exothermic peak height was observed with prolonged humidification times (Fig. 7b).

The layer thickness with the original lead screw was  $87.2 \pm 2.0 \mu\text{m}$ , while the reduced layer thickness was  $43.7 \pm 2.7 \mu\text{m}$ .

Prior to presenting the statistical analysis of the various results gathered in this study it must be underlined that the results of samples for printed with powders humidified for 20 s were excluded from the statistical analysis. Indeed, some of the 3DP specimens could not be individually extracted from the powder bed because most of the powder bed was glued together as a single

mass. This observation was made for all series combining the 20 s moisture regime and 12 printed samples. This glueing effect was never found in the absence of humidification or at the low moisture application time of 5 s. For 10 s humidification it occurred only once (12 printed samples and 88  $\mu\text{m}$  layer thickness).

Apart from two exceptions (the inner circle and cube length), the layer thickness played a significant role for all aspects investigated here. In particular, the surface roughness increased significantly with an increase in layer thickness ( $P < 0.01$ , mean roughness of all results 45  $\mu\text{m}$ , effect of layer thickness 8.5  $\mu\text{m}$ ,

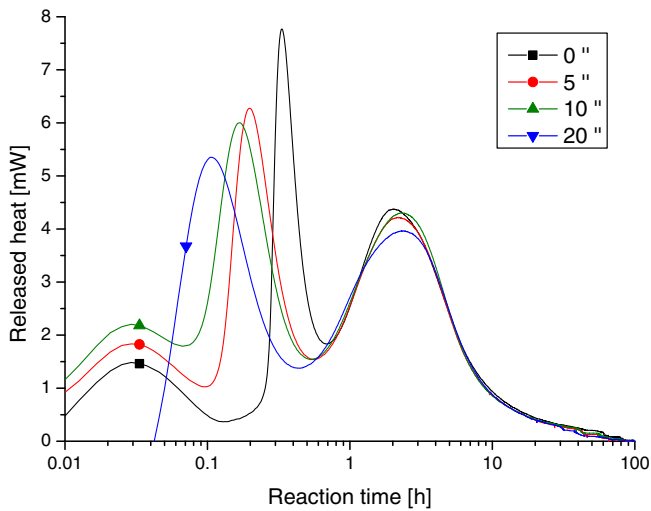


Fig. 6a. Heat released from humidified  $\alpha$ -TCP in sodium phosphate solution.

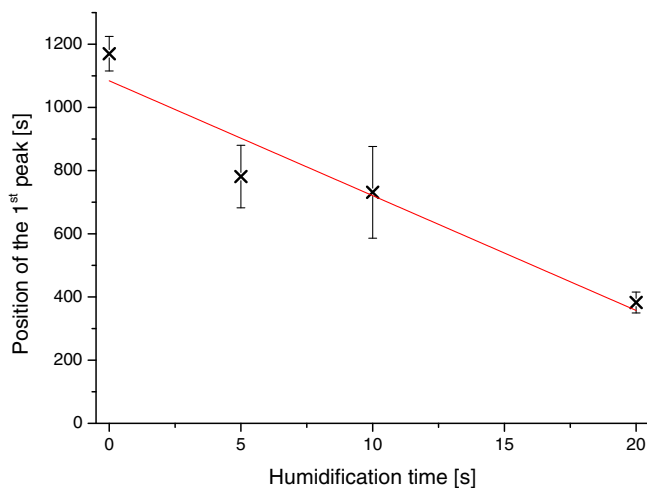


Fig. 6b. Position of the first peak of heat released from humidified  $\alpha$ -TCP in sodium phosphate solution ( $R^2 = 0.9$ ).

Table 2). Similarly, the statistical analysis revealed a significant effect ( $P < 0.01$ ) of a change in layer thickness on the size of the sphere outer circle (mean 10.93 mm, effect  $-0.18$  mm), cylinder length (mean 10.92 mm, effect  $-0.16$  mm), cylinder height (mean 5.60 mm, effect  $-0.18$  mm) and cylinder angle (mean  $0.79^\circ$ , effect  $-0.56^\circ$ , Table 2). More complex and numerous effects were seen for the cube height and cube angle, as presented in Fig. 8. For the cube height a significant interaction ( $P < 0.01$ ) between layer thickness, number of printed specimens and humidification time was detected. Specifically, it was observed that the printing accuracy was poor with the combination small layer thickness–low humidification time–low number of printed samples. All other conditions led to dimensions slightly larger than 10 mm, the nominal value.

Similar observations were made for the cube angle results. Large cube angles resulted from powder bed displacements due to recoating by the counter-rotating roller. In general the absolute angle value decreased with an increase in humidification time at a layer thickness of  $44 \mu\text{m}$ . Almost perfect accuracies (angle values close to zero) were obtained for scaffolds printed at a layer thickness of  $88 \mu\text{m}$ .

In the present study only a few results were simultaneously affected by the factors layer thickness and humidification. However, humidification did not induce any significant improvement, be-

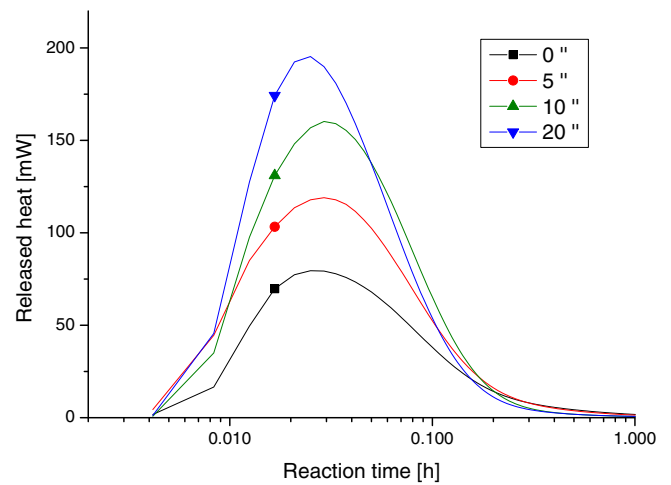


Fig. 7a. Heat released from humidified  $\alpha$ -TCP in water and MCPM.

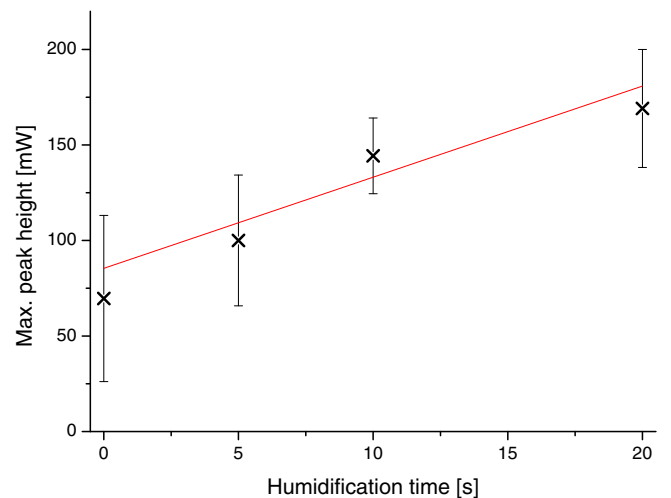


Fig. 7b. Maximal peak height for humidified  $\alpha$ -TCP in water and MCPM ( $R^2 = 0.6$ ).

cause the significance level was set very low ( $P < 0.01$ ). The interaction between layer thickness and humidification time was, however, significant at a level of  $P = 0.021$ . Specifically, the surface roughness of samples printed with  $44 \mu\text{m}$  layers was reduced from  $43$  to  $29 \mu\text{m}$  with an increase in humidification time, whereas the opposite was measured for  $88 \mu\text{m}$  layers, with an increase from  $46$  to  $60 \mu\text{m}$  (Supplementary Fig. S1).

In this study the printing accuracy of the machine corresponded to the nominal value of  $300 \times 450$  dpi ( $85 \times 65 \mu\text{m}$ ). However, in fact, the height difference between peaks and valleys measured with the surface roughness analysis system was often larger than  $200 \mu\text{m}$ , even for a layer thickness of  $88 \mu\text{m}$  (Fig. 9). Determination of the dynamic print head positioning errors during 3DP was not feasible since the nozzle used could change for every layer. However using ZCorp low level commands the print head can be controlled to approach a given pair of coordinates. Quantification of the (static) positioning accuracy was found to be fairly high (around  $4 \mu\text{m}$ ) using an external laser sensor (Micro Laser Sensor LM10, NAI, Matsushita, Japan).

#### 4. Discussion

In this study the relation between different 3DP parameters and the final printing outcome was assessed. For that purpose the same powder and 3DP settings were used in order to elaborate the ef-

**Table 2**

Significant ( $P < 0.01$ ) effects of factors and interactions of factors (e.g. AC designates interaction between factors A and C).

Measure	Significance ( $P$ value)	Mean	Target value	Effect
Sphere outer circle	A (0.0041)	10.93 mm	10 mm	-0.18
Cylinder length	A (0.0029)	10.92 mm	10 mm	-0.16
Cylinder height	A (0.0016)	5.60 mm	5 mm	-0.18
Cylinder angle	A (0.0009)	0.79°	0°	-0.56
Cube height	A (0.0001)	10.00 mm	10 mm	0.54
	B (<0.0001)			-0.69
	AB (<0.0001)			0.60
	C (0.0005)			0.54
	AC (0.0016)			-0.47
	BC (0.0001)			0.65
	ABC (0.0003)			-0.58
	Cube angle (°)	A (0.0003)	3.74°	0°
	B (0.0070)			2.18
	AB (0.0072)			-2.17
	C (0.0057)			2.76
	AC (0.0040)			2.92
Surface roughness	A (0.0021)	44.9 $\mu$ m		8.5

The three investigated factors were: factor A, layer thickness, 44 and 88  $\mu$ m; factor B, part number, 6 and 12 parts; factor C, humidification time, 0, 5 and 10 s. The mean corresponds to the mean value of all results for the given response (e.g. mean length of all cylinders 10.92 mm). The effect is the effect of the factor considered in the table.

fects of three selected parameters: (i) layer thickness, 44 vs. 88  $\mu$ m; (ii) number of printed pieces, 6 vs. 12; (iii) humidification time, 0, 5, 10 and 20 s.

According to a previous study [18] promising 3DP results for a layer thickness of 88  $\mu$ m can be expected for mean particle sizes in the range 20–35  $\mu$ m, compaction rate  $\rho_{\text{Tapped}}/\rho_{\text{Bulk}}$  in the range 1.3–1.4, flowability ( $ff_c$  value) in the range 5–7 and powder bed surface roughness ( $S_a$ ) of 10–25  $\mu$ m. The characteristics of the powder used in this study (mean particle size  $\sim$ 21  $\mu$ m, compaction rate 1.44, flowability 5) were very close, with only the compaction rate being slightly higher than the target range.

Instead of focussing on the powder bed surface, as done in a previous study [18], the surface roughness and geometrical accuracy of the final printed samples were investigated here. These parameters are less difficult to measure than the powder bed surface roughness and are more relevant to assess the final 3DP outcome. Nevertheless, a single surface roughness of the powder bed with the powder used in this study resulted in a value of  $10.99 \pm 1.15$   $\mu$ m. This value is at the lower limit of the values obtained in Butscher et al. [18] (10–25  $\mu$ m), and thus promising 3DP results can be expected.

In this study the focus was on the relationship between layer thickness and printing accuracy using the same powder. Since it is known that the powder properties must be optimized for a given layer thickness, the choice of powder used here had to be critically considered. The selected powder was chosen for two reasons. Firstly, good printing results have been obtained with this powder using a layer thickness of 88  $\mu$ m [18]. Secondly, it was not clear what parameters the powder should have to be optimal for a layer thickness of 44  $\mu$ m. There are conflicting requirements between good flowability (particles > 20  $\mu$ m), on the one hand, and the need for a limited particle size due to a given layer thickness, on the other.

Printing thinner layers implies the use of higher shear forces during recoating. To stabilize the powder bed an approach mentioned by the inventors of 3DP was used [30]. The use of pure water moisture is believed to stabilize the top powder bed layer through the formation of liquid bridges between particles. It is known that capillary effects can lead to rearrangement of fine pow-

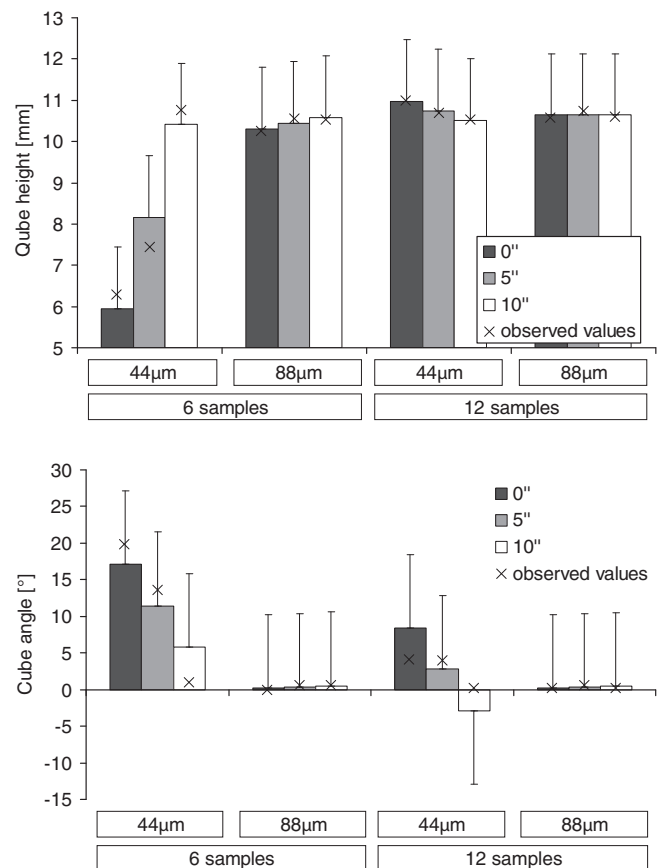


**Fig. 8.** Dependency of cube height (above) and angle (below) on layer thickness (44 and 88  $\mu$ m) and number of printed samples (6 vs. 12 samples). The symbols (x) correspond to the mean values of the measured data. The columns correspond to the adjusted values according to the statistical model and the error bars to the 99% confidence intervals.

ders [45]. Thus the amount of moisture must be carefully tailored. Since our results showed that a 20 s humidification time was too long, the selected humidification times (0, 5, 10 and 20 s) were in the relevant range.

Moisture application or humidification has the advantage of leaving no residues. However  $\alpha$ -TCP is known to react with water [46,47]. For this reason the build volume was always placed in a furnace at 200 °C for 1 h immediately after printing the final layers to minimize the water interaction. Reduced reactivity was expected after reaction of  $\alpha$ -TCP with water droplets. Calorimetry results revealed even higher and faster reactivity of  $\alpha$ -TCP after humidification (and drying at 200 °C for 1 h) compared with the untreated powder (Figs. 6 and 7). The higher initial reactivity might be related to the formation of fine crystalline structures on the surface (apatite nuclei), while leaving most of the powder particles unreacted (Fig. 5). Therefore, 3DP with recycled powder is not only possible but beneficial, since high reactivity promotes early mechanical stability of the printed parts.

Statistical analysis of the effects of the three factors investigated on the geometrical accuracy of printed samples (cubes, cylinders and spheres) is summarized in Table 2. Based on published data [48] it was assumed that geometrical changes in the printed samples are not due to setting reaction-related dimensional changes but rather are a result of 3DP factors, as discussed below. In general, an increase in the layer thickness from 44 to 88  $\mu$ m led to a decrease in the investigated response. Since the mean values of the tested responses were high (e.g. the projected outer circle of the sphere had a mean size of 10.93 mm whereas the nominal va-

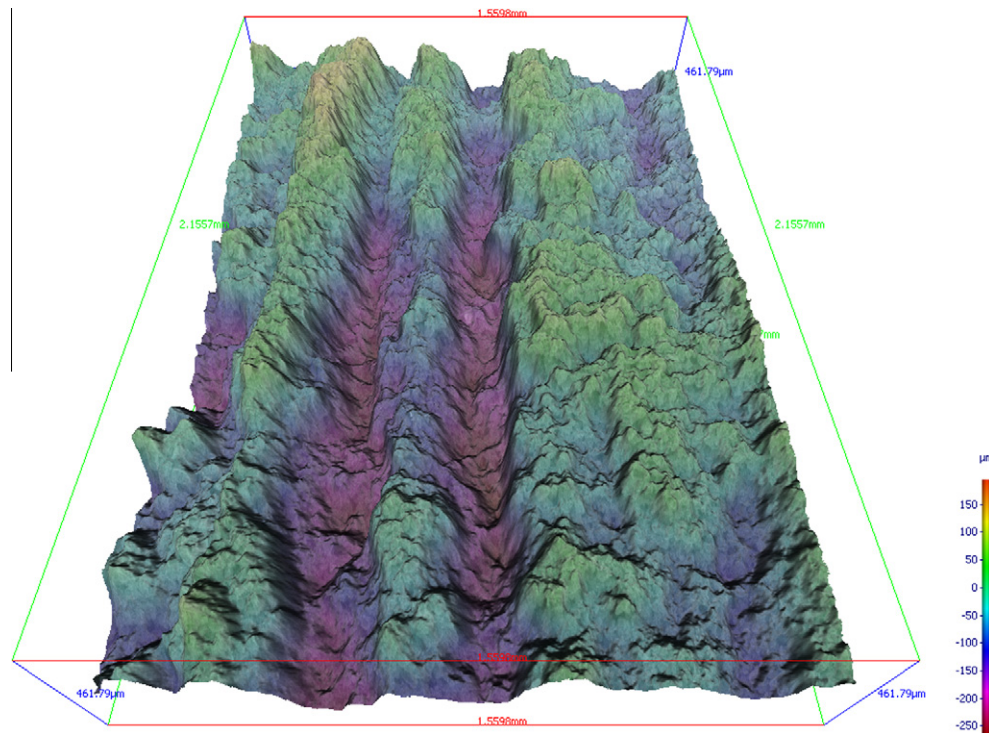


Fig. 9. Surface roughness profile of a 3DP specimen with a layer thickness of 88  $\mu\text{m}$ .

lue was 10.00 mm), increasing the layer thickness had a positive effect on the printing accuracy. These results can be explained by the fact that it was often more difficult to obtain good printing results with thinner layer thicknesses due to stronger shear forces.

More complex results were obtained for the cube height and cube angle. In both cases multiple interactions were observed between the three factors investigated. Despite multiple interactions, the outcome was fairly clear, with the values for cube height and cube angle being far from the nominal values (10 mm and  $0^\circ$ ) for a  $44 \mu\text{m}$  layer thickness, six printed parts, and an absence of humidification. This result implies two important conclusions: First, printing twelve pieces instead of six stabilized the printing bed and enhanced printing accuracy. Second, the use of a short humidification time was an effective approach to print pieces with a thinner layer thickness.

Regarding the positive effect of an increase in the number of printed pieces on the printing accuracy, it is interesting to note that the last cube layers were especially critical. Since the cubes were the highest printed specimen (no neighbouring printed layers), this result again underlines the link between printing accuracy/powder bed stability and the number of printed specimens. Printing six specimens with a layer thickness of  $44 \mu\text{m}$  and no humidification always resulted in damaged printed parts due to displacement in the direction of roller movement. Some of these damaged parts resulted in extreme geometrical values. This is of course not acceptable and might result in major damages when printing more porous scaffolds. While for 5 s moisture application this effect was lower, but still present, for higher (10 s) moisture times no displacement could be detected, with resultant stabilization of the powder bed. To sum up, it can be stated that the combination of a greater layer thickness and a high printing density (twelve printed parts) yielded the best geometrical accuracy, while humidification had no significant effect. For thin layer thicknesses humidification enhanced the geometrical accuracy, especially when no neighbouring support by other specimens was available, which might be of special relevance for the complex architectural features of scaffolds.

Looking at the surface roughness results (Table 2), it appears that significantly lower roughness values were obtained with a  $44 \mu\text{m}$  layer thickness. Theoretically the thinner the powder layer the higher the resolution. The difference in surface roughness provoked by a change in layer thickness was small ( $8.5 \mu\text{m}$ ) compared with the change in layer thickness ( $44 \mu\text{m}$ ). The benefit of small stair steps was negligible or irrelevant if these small stair steps were inaccurate. This inaccuracy could be related to: (i) print head positioning; (ii) binder deposition errors; (iii) binder wicking; (iv) powder bed instability. Print head positioning errors are inevitable due to positioning errors of the linear stage carrying the print head. Even if print head positioning is perfect, binder drops may deviate from their optimal target during flight and possibly also form small satellite droplets. Based on the results concerning print head positioning, it is expected that binder wicking as well as powder bed instability during 3DP play dominant roles in printing accuracy. The impact of binder wicking or bleeding into neighbouring powder particles due to capillary effects is difficult to quantify [1]. The effect of powder bed stability and the resulting accuracy errors due to shear forces during recoating are discussed in this paper. An enhanced understanding of all these non-trivial error sources as well as their interactions might enable substantially higher printing accuracy.

Considering the final goal of printing macroporous scaffolds, depowdering needs to be taken into account. To enable depowdering it appears beneficial to have a combination of high geometrical accuracy and a small surface roughness, which in the present study is possible only for the combination of thin layer thickness, high batch density and humidification. The stabilizing effect of a high printing density in the build volume suggests that printing auxiliary support structures around specimens of critical shape could further enhance the geometric accuracy.

## 5. Conclusion and outlook

In conclusion, this study looked at the interplay between layer thickness, moisture application and the final printing outcome of 3DP using a powder optimized for an  $88 \mu\text{m}$  layer thickness. A

reduction in the layer thickness to 44  $\mu\text{m}$  was shown to be the most critical factor for powder bed stability, but allowed the lowest surface roughness. A lack of powder bed stability resulted in partly or fully damaged specimens. Humidification was found to improve the powder bed stability and printing accuracy, enabling 3DP with a 44  $\mu\text{m}$  layer thickness even with a powder not specifically optimized for 44  $\mu\text{m}$ . In the light of the time-intensive preparation of the very narrowly distributed powder fractions necessary for 3DP, this is a promising insight for 3DP research. Furthermore, the benefit of humidification was not detrimental concerning reactivity. Surprisingly, the recycled humidified  $\alpha$ -TCP powder was more reactive than the non-humidified counterpart. Taking into account the labour-intensive and costly preparation of powders for 3DP this fact becomes even more relevant.

While accuracy and surface roughness are critical factors for the simple solids analysed in this study, they are even more critical for complex and porous scaffolds. Therefore, moisture-based 3DP is believed to be a promising approach for high resolution 3DP based scaffold engineering.

### Acknowledgements

Funding from the RMS Foundation is gratefully acknowledged. The authors express their appreciation to F. Bigolin of the RMS Foundation for SEM analysis.

### Appendix A. Figures with essential colour discrimination

Certain figures in this article, particularly Figs. 1, 2, 4, 6, 7 and 9, are difficult to interpret in black and white. The full colour images can be found in the on-line version, at <http://dx.doi.org/10.1016/j.actbio.2012.10.009>.

### Appendix B. Supplementary data

Supplementary data associated with this article can be found, in the online version, at <http://dx.doi.org/10.1016/j.actbio.2012.10.009>.

### References

- Butscher A et al. Structural and material approaches to bone tissue engineering in powder-based three-dimensional printing. *Acta Biomater* 2011;7(3):907–20.
- Klammert U et al. 3D powder printed calcium phosphate implants for reconstruction of cranial and maxillofacial defects. *J Craniomaxillofac Surg* 2010;38(8):565–70.
- Hänel T et al. Aus CT-Daten generierte patientenindividuelle Implantate aus  $\beta$ -Tricalciumphosphat für die Knochenregeneration. *Z Regen Med* 2009;2(1):13–7.
- Peters F et al. Comparative study of patient individual implants from beta-tricalcium phosphate made by different techniques based on CT data. *Materialwiss Werkstofftech* 2006;37(6):457–61.
- Constantz BR et al. Skeletal repair by in situ formation of the mineral phase of bone. *Science* 1995;267(5205):1796–9.
- Dorozhkin SV. Bioceramics of calcium orthophosphates. *Biomaterials* 2010;31(7):1465–85.
- Bohner M. Calcium orthophosphates in medicine: from ceramics to calcium phosphate cements. *Injury* 2000;31(Suppl. 4):37–47.
- Moseke C, Gbureck U. Tetra-calcium phosphate: synthesis, properties and biomedical applications. *Acta Biomater* 2010;6(10):3815–23.
- Yeong WY et al. Rapid prototyping in tissue engineering: challenges and potential. *Trends Biotechnol* 2004;22(12):643–52.
- Detsch R et al. In vitro-osteoclastic activity studies on surfaces of 3D printed calcium phosphate scaffolds. *J Biomater Appl* 2011;26(3):359–80.
- Habibovic P et al. Osteoconduction and osteoinduction of low-temperature 3D printed bioceramic implants. *Biomaterials* 2008;29(7):944–53.
- Klammert U et al. Cytocompatibility of brushite and monetite cell culture scaffolds made by three-dimensional powder printing. *Acta Biomater* 2009;5(2):727–34.
- Bohner M et al. Commentary: deciphering the link between architecture and biological response of a bone graft substitute. *Acta Biomater* 2011;7(2):478–84.
- Karageorgiou V, Kaplan D. Porosity of 3D biomaterial scaffolds and osteogenesis. *Biomaterials* 2005;26(27):5474–91.
- LeGeros RZ. Properties of osteoconductive biomaterials: calcium phosphates. *Clin Orthop Relat Res* 2002;395:81–98.
- Bohner M et al. Synthesis and characterization of porous beta-tricalcium phosphate blocks. *Biomaterials* 2005;26(31):6099–105.
- Maier AK et al. Three-dimensional printing of flash-setting calcium aluminate cement. *J Mater Sci* 2011;46(9):2947–54.
- Butscher A et al. Printability of calcium phosphate powders for three-dimensional printing of tissue engineering scaffolds. *Acta Biomater* 2012;8(1):373–85.
- Melcher R. Rapid Prototyping von Keramiken durch 3D-Drucken. In: *Lehrstuhl Glas und Keramik*. Erlangen, Germany: Universität Erlangen-Nürnberg; 2009.
- Spillmann A, Sonnenfeld A, von Rohr PR. Flowability modification of lactose powder by plasma enhanced chemical vapor deposition. *Plasma Processes Polym* 2007;4:S16–20.
- Utela BR. Development and application of new material systems for three dimensional printing (3DP). St Louis, MO: University of Washington; 2008.
- Roth C et al. Plasma surface modification of powders for pharmaceutical applications. *Surf Coat Technol* 2011;205:S597–600.
- Zimmermann I, Eber M, Meyer K. Nanomaterials as flow regulators in dry powders. *Z Phys Chem* 2004;218(1):51–102.
- Butscher A et al. Printability of calcium phosphate powders for three-dimensional printing of tissue engineering scaffolds. *Acta Biomater* 2012;8(1):373–85.
- Will J et al. Porous ceramic bone scaffolds for vascularized bone tissue regeneration. *J Mater Sci: Mater Med* 2008;19(8):2781–90.
- Bergmann C et al. 3D printing of bone substitute implants using calcium phosphate and bioactive glasses. *J Eur Ceram Soc* 2010;30(12):2563–7.
- Shanjani Y et al. Modeling and characterization of biomaterials spreading properties in powder-based rapid prototyping techniques. In: *ASME international mechanical engineering congress and exposition*, Seattle, WA, US: American Society of Mechanical Engineers; 2007.
- Shanjani Y et al. Mechanical characteristics of solid-freeform-fabricated porous calcium polyphosphate structures with oriented stacked layers. *Acta Biomater* 2011;7(4):1788–96.
- Sachs E et al. Three dimensional printing: the physics and implications of additive manufacturing. *CIRP Ann* 1993;42:257–60.
- Cima M et al. Three-dimensional printing techniques; 1995. US Patent US5387380.
- Merten HA et al. Intraindividual comparative animal study of alpha- and beta-tricalcium phosphate degradation in conjunction with simultaneous insertion of dental implants. *J Craniofac Surg* 2001;12(1):59–68.
- Gbureck U et al. Preparation of tricalcium phosphate/calcium pyrophosphate structures via rapid prototyping. *J Mater Sci: Mater Med* 2008;19(4):1559–63.
- Rodriguez-Carvajal J. Recent developments of the program FULLPROF. *Commission Powder Diffr Newslett* 2001;26:12–9.
- Dickens B, Schroeder LW, Brown WE. Crystallographic studies on the role of Mg as a stabilizing impurity in  $\beta$ - $\text{Ca}_3(\text{PO}_4)_2$ . I. The crystal structure of pure  $\beta$ - $\text{Ca}_3(\text{PO}_4)_2$ . *J Solid-State Chem* 1974;10:232–48.
- Sudarsanan K, Young RA. Significant precision in crystal structure details: Holly Springs hydroxyapatite. *Acta Crystallogr* 1969;B25:1534–43.
- Boudin S et al. Redetermination of the  $\beta$ - $\text{Ca}_2\text{P}_2\text{O}_7$  structure. *Acta Crystallogr C* 1993;49(12):2062–4.
- Mathew M et al. Crystal-structure of alpha- $\text{Ca}_3(\text{PO}_4)_2$ . *Acta Crystallogr B* 1977;33:1325–33.
- Schulze D. Flowability of bulk solids – definition and measuring principles. *Chem Ing Tech* 1995;67(1):60–8.
- Nebelung M, Lang B. Flowability of ceramic bulk materials part 1: methods. *Ceram Forum Int* 2009;86(3):E35–40.
- Nebelung M, Lang B. Flowability of ceramic bulk materials part 2: interaction of primary particle properties and flowability. *Ceram Forum Int* 2009;86(4):E35–8.
- Schulze D, Wittmaier A. Flow properties of highly dispersed powders at very small consolidation stresses. *Chem Eng Technol* 2003;26(2):133–7.
- Kurt K. Aerosil zur Verbesserung des Fließverhaltens pulverformiger Substanzen. In: *Schriftenreihe Pigmente*, vol. 31. Frankfurt/M: Degussa; 1981. p. 1–20.
- DIN EN 725–8: advanced technical ceramics – methods of test for ceramic powders – part 8: determination of tapped bulk density. 2006. Available from: <http://www.beuth.de/langanzeige/DIN-EN-725-8/de/88828024.html&bcrumblelevel=4&SearchID=282576440>.
- DIN EN 725–9: advanced technical ceramics – methods of test for ceramic powders – part 9: determination of tapped bulk density. 2006 Available from: <http://www.beuth.de/langanzeige/DIN-EN-725-9/de/88827999.html&bcrumblelevel=3&SearchID=282577090>.
- Lanzetta M, Sachs E. Improved surface finish in 3D printing using bimodal powder distribution. *Rapid Prototyping J* 2003;9(3):157–66.
- Monma H, Kanazawa T. The hydration of alpha-tricalcium phosphate. *J Ceram Soc Jpn* 2000;108(8):S75–80.
- Driessens FCM et al. Effective formulations for the preparation of calcium-phosphate bone cements. *J Mater Sci: Mater Med* 1994;5(3):164–70.
- Fernandez E et al. Dimensional and thermal behavior of calcium-phosphate cements during setting compared to PMMA bone cements. *J Mater Sci Lett* 1995;14(1):4–5.

**Update**

**Acta Biomaterialia**

Volume 9, Issue 11, November 2013, Page 9242

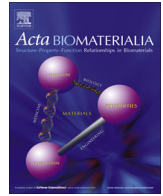
DOI: <https://doi.org/10.1016/j.actbio.2013.07.006>



Contents lists available at ScienceDirect

Acta Biomaterialia

journal homepage: [www.elsevier.com/locate/actabiomat](http://www.elsevier.com/locate/actabiomat)



Erratum

Errata to: “Moisture based three-dimensional printing of calcium phosphate structures for scaffold engineering” [Acta Biomaterialia 9 (2013) 5369–5378]



A. Butscher<sup>a,b,\*</sup>, M. Bohner<sup>a</sup>, N. Doebelin<sup>a</sup>, L. Galea<sup>a</sup>, O. Loeffel<sup>a</sup>, R. Müller<sup>b</sup>

<sup>a</sup>RMS Foundation, Bischmattstrasse 12, CH-2544 Bettlach, Switzerland

<sup>b</sup>Institute for Biomechanics, ETH Zurich, Wolfgang-Pauli-Strasse 10, CH-8093 Zurich, Switzerland

The publisher regrets the error on page 1, under Abstract, third sentence. The correction is listed below as it should have appeared: However, 3DP has major limitations, such as limited resolution and accuracy, hence preventing the widespread application of this method within scaffold engineering.

DOI of original article: <http://dx.doi.org/10.1016/j.actbio.2012.10.009>

\* Corresponding author at: RMS Foundation, Bischmattstrasse 12, CH-2544 Bettlach, Switzerland. Tel.: +41 32 644 1400; fax: +41 32 644 1176.  
E-mail address: [andre.butscher@rms-foundation.ch](mailto:andre.butscher@rms-foundation.ch) (A. Butscher).